Click Here for Full Article

Multistation observations of ELF/VLF whistler mode chorus

M. Gołkowski[1] and U. S. Inan[1]

[1] An array of seven ELF/VLF receivers in Alaska is utilized for direction finding and determination of ionospheric exit point of whistler mode chorus waves from the Earth's magnetosphere. Each receiver records both orthogonal horizontal magnetic components of the chorus waves. All sites use GPS-synchronized sampling, allowing for the localization of ionospheric exit points utilizing both arrival azimuth and time of arrival lag between sites. Results show two distinct groups of cases, emissions with singular ionospheric exit points and those with multiple exit points. Singular exit point cases exhibit migration and mode conversion as a function of propagation distance from the source point. The multiple exit point case shows chorus waves impinging on the ionosphere over a spread in magnetic latitude, suggesting nonducted propagation. Ray tracing for this case is unable to reproduce the observations unless a cold plasma density different than that predicted by geomagnetic conditions is used. It is proposed that chorus elements cross the transionospheric boundary after experiencing scattering from meter-scale irregularities. Additionally, subionospheric VLF remote sensing is used to detect precipitation onto the ionosphere of energetic radiation belt electrons that have been pitch angle scattered by individual chorus emission packets. VLF perturbation signatures are consistent with precipitation fluxes being dominated by electrons with energies less than 1 MeV.

Citation: Gołkowski, M., and U. S. Inan (2008), Multistation observations of ELF/VLF whistler mode chorus, *J. Geophys. Res.*, *113*, A08210, doi:10.1029/2007JA012977.

1. Introduction

[2] As one of the most intense natural magnetospheric radio emissions, whistler mode chorus has been extensively observed and studied since the first report by *Storey* [1953], who gave these emissions their name because of their characteristic sound resembling a "rookery" when played through a speaker. Chorus waves are characterized by sequences of usually rising, less often falling, repeating, narrowband tones in the frequency range of a few hundred hertz to several kHz (see review by *Sazhin and Hayakawa* [1992]). Although there is general agreement that chorus generation occurs as a result of gyroresonance between radiation belt electrons and VLF waves, the source mechanism and chorus properties are still subjects of active experimental and theoretical research [*Lauben et al.*, 2002; *Inan et al.*, 2004; *Bortnik et al.*, 2007; *Santolík and Gurnett*, 2003].

[3] Of the multitude of ground observations of chorus in the literature, relatively few studies present quantitative treatment of multiple station observations or direction-finding measurements of the arrival direction of chorus or other magnetospheric emissions. *Carpenter* [1980] performed direction finding on signals from the Siple Station transmitter and found unexpected fast variations in ampli-tude and arrival azimuth that were qualitatively attributed to drifts of low-energy "clouds" of electrons through a pattern of whistler ducts. *Strangeways et al.* [1982] used triangulation of whistler exit points with four stations in Canada and found a discrepancy between the *L* shell values of the triangulated exit points and those calculated from whistler nose frequencies. This discrepancy was explained to be the result of "unducting" of the signals at 1000 km altitude and subsequent refraction through the ionosphere. *Tsuruda et al.* [1982] reported high spatial attenuation (∼7 dB/100 km) and identified changing active zones of chorus activity. Most notably, *Madden et al.* [1978] found distinct exit points of chorus risers in the 1.0–1.4 kHz frequency range using direction-finding triangulations from two stations in Iceland. Conventionally, chorus emissions observed on the ground are believed to have traveled in magnetospheric density enhancements or "ducts" [*Sazhin and Hayakawa*, 1992]. However, current theoretical studies [*Bortnik et al.*, 2007; *Chum and Santolík*, 2005] and the results presented herein suggest that nonducted emissions are also present in ground observations. Earlier studies were hindered by the lack of timing accuracy between stations and had to rely primarily on direction-finding techniques, which often led to uncertainties in triangulated position on the order of hundreds of kilometers [*Hayakawa et al.*, 1981]. The primary tool for direction finding was the crossed loop goniometer, although more complicated devices and algorithms were also developed that incorporated a vertical electric monopole [*Leavitt et al.*, 1978; *Tsuruda and Hayashi*,

---

[1]STAR Laboratory, Stanford University, Stanford, California, USA.
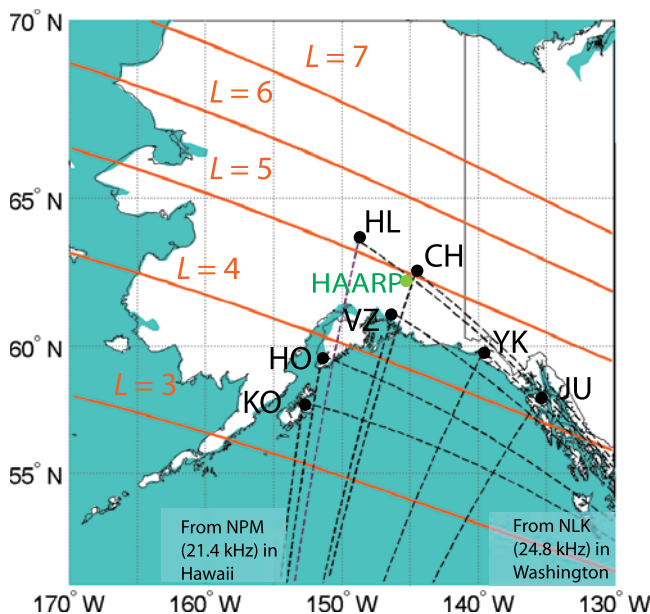
Figure 1. Map showing seven receivers in Alaska in Chistochina (CH), Valdez (VZ), Homer (HO), Healy (HL), Kodiak (KO), Yakutat (YK), and Juneau (JU) as well as the location of the High frequency Active Auroral Research Program (HAARP) high-frequency heating facility. Dashed lines represent great circle paths of the signals from the two nearest VLF transmitters, NLK in Washington state and NPM in Hawaii.

1974; *Cousins*, 1972]. Advancements in timing accuracy facilitated by the Global Positioning System (GPS) have made multistation observations more relevant since exact time delays and phase differences can now be calculated and used as a complement to arrival bearing in triangulation of emissions.

[4] The role of chorus in the precipitation of radiation belt electrons has been studied both theoretically and observationally. Modeling of cyclotron resonant wave-particle interactions suggests that the energy range of particles precipitated spans a wide range from tens of keV to more than 1 MeV [*Bortnik and Thorne*, 2007]. Understanding the loss and acceleration mechanisms of energetic electrons is a key to radiation belt dynamics in which chorus waves are believed to be play a major role. Satellite observations analyzed by *Lorentzen et al.* [2001] were found to show a correspondence between relativistic electron microbursts and individual chorus elements; however, the relationship was based primarily on the similarity of time signatures and their distribution in local time and was not one to one. In a study of electron acceleration processes, *O'Brien et al.* [2003] found further evidence of a local time correspondence between microbursts and chorus waves and actually used microburst observations as a proxy for chorus wave activity. *Rosenberg et al.* [1981] showed a correlation between ground-based chorus measurements and X-ray bursts observed on a balloon. VLF remote sensing using subionospherically propagating radio signals to detect ionospheric perturbations is one of the few methods of detecting energetic electron precipitation over a wide energy range and across large geographic scales. This technique has been

used for many years to probe the ionosphere and more recently to detect precipitation induced by lightning [*Peter and Inan*, 2004, and references therein] or man-made VLF transmitters [*Inan et al.*, 2007]. If the exit points of individual chorus elements can be accurately located, the VLF remote sensing technique can serve as a valuable tool in quantifying chorus-induced precipitation. Using VLF remote sensing, *Dingle and Carpenter* [1981] showed a one-to-one correspondence between whistler-triggered chorus events and ionospheric perturbations. In a recent study, *Rodger et al.* [2007] present observations which the authors claim show only high-energy (>1 MeV) electron precipitation signatures and the absence of the lower-energy electron precipitation. Such a conclusion is contrary to most modeling work on wave-particle interactions and other observations, including those presented in this work, but it shows some agreement with satellite measurements.

[5] In this study we examine chorus data recorded at multiple stations synchronized with GPS timing. By accurately determining chorus magnetospheric exit points for the first time, we are able to infer propagation characteristics of the chorus in the magnetosphere. Additionally, we show subionospheric perturbations caused by chorus-induced electron precipitation.

2. Experimental Setup and Methodology

2.1. Location and Hardware

[6] The observations presented in this study were made with an array of ELF/VLF receivers in Alaska. Figure 1 shows a map of the seven receiver stations as well as lines of constant L value and the great circle paths of signals from the two nearest U.S. Navy VLF transmitters. The ELF/VLF receivers were of the Atmospheric Weather Electromagnetic System for Observation Modeling and Education design developed by Stanford University and now being deployed worldwide in the context of International Heliophysical Year 2007. The receivers utilized two orthogonal large square (4.8 m × 4.8 m) or triangular (4.2 m high with 8.4 m base) air core loop antennas matched to a low-noise preamplifier with flat frequency response (~300 Hz to ~47 kHz). Recordings were made in both broadband mode (digital sampling at 100 kHz) and narrowband mode (50 Hz digital sampling of 200 Hz band around VLF transmitter signals with real-time demodulation of amplitude and phase). All digital sampling was synchronized to GPS timing signals, allowing for 200 ns timing accuracy between all stations.

2.2. Analysis Method

[7] The advantage of GPS-synchronized multisite observations is that cross correlations of the same chorus emission at different sites can be performed to determine the time of arrival lag. Curves of constant time of arrival lag between different pairs of sites, along with arrival azimuth from each site, allow for the geolocation of the ionospheric exit points (or the points at which the wave packet enters the Earth-ionosphere waveguide) of the chorus emissions. Time of arrival analysis has been used with success for geolocation of "sferics" in the VLF band [*Lee*, 1986] and even for Pc1-2 pulsations in the ULF band [*Neudegg et al.*, 1995] by calculating a cross correlation and hence the time lag of
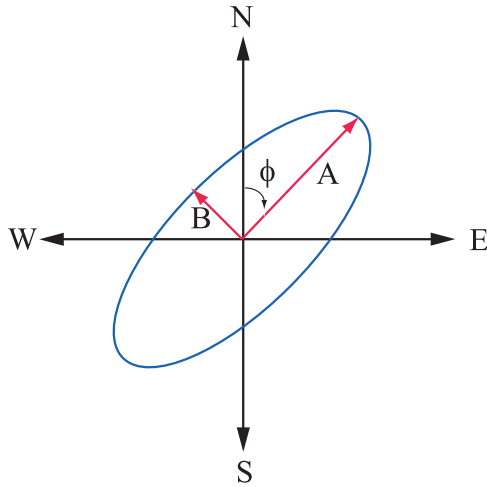
Figure 2. Generalized polarization ellipse for field vectors of electromagnetic waves. N-S and E-W represent antennas oriented in geographic north-south and east-west directions.

the signals between two sites. Unfortunately, because of the limited bandwidth of chorus, which is at most a few kHz, cross correlation of even identical emissions yields a $\sin(x)/x$ envelope instead of the Dirac delta function expected for cross correlation of signals with large bandwidths. Such a cross-correlation signature is sensitive to noise and interference, making adequate signal-to-noise ratios necessary requirements of the technique. In our analysis, after the identification of chorus emissions at multiple stations, the individual chorus elements are isolated by passing the data through a digital bandpass filter with passband equal to the frequency range of the emissions, typically $0.5–4$ kHz. Interference of 60 Hz power line harmonics is removed using a second digital filter with stop bands at the identified frequencies. The same filters are applied to data from all stations so that relative phase is preserved. In general, at a receiver, the wavefield of a whistler mode signal exiting the ionosphere will be composed of the summation of a number of rays or a number of waveguide modes. If the distance along the ground from the receiver to directly below the exit point is less than the ionospheric height ($\sim$85 km), then a single direct ray is dominant [*Yearby and Smith*, 1994]. For sites at distances greater than 85 km but less than 1000 km from the exit point, the rays received will include the direct ray as well as rays that have undergone multiple reflections from the Earth and lower ionospheric boundary [*Yearby and Smith*, 1994]. The phase, polarization, and arrival time of each ray will be different and will depend on the number of reflections experienced. Time of arrival differences between stations are only meaningful if individual rays can be identified and their propagation path (i.e., number of reflections) can be determined. Our approach is to identify the direct ray at each station, which is possible since, for the direct ray only, the maximum time of arrival lag between two stations is bounded by the ground distance between the two stations divided by the free space propagation speed. In fact, the cross correlation of a direct ray with a nondirect ray will always yield a time of arrival lag greater than this direct ray to direct ray upper bound. Additionally, the unique elevation angle and the general elliptical polarization of each ray,

which is discussed further below, create a unique phasing of the horizontal magnetic field of each ray. Each station records two orthogonal components of the wave horizontal magnetic field, B_{NS} and B_{EW}. Through the following simple trigonometric relation it is possible to obtain the horizontal magnetic field in any arbitrary direction (θ) measured in degrees east of north.

$$B(\theta) = B_{NS}\cos(\theta) + B_{EW}(t)\sin(\theta) \quad (1)$$

[8] For each two-station pair with identified chorus elements, the filtered data are cross correlated for all combinations of θ from $-90°$ to $90°$ for each site. Only if the cross-correlation coefficient is greater than 0.5 and the time lag is less than the direct ray upper bound is the time lag accepted as a time of arrival difference for direct rays. In practice it is found that the cross-correlation time lags are largely independent of the chosen θ for a station closer to the exit point and show variation primarily for the more distant station, as expected.

[9] Measurements of two orthogonal components of the magnetic field of a wave propagating in the Earth-ionosphere waveguide allow for an estimate of the arrival azimuth by determination of the general polarization ellipse. Figure 2 shows the polarization ellipse with reference to the two antennas oriented orthogonally in the geographic north-south (NS) and east-west (EW) directions. If we combine the time domain inputs from the two antennas as follows:

$$f(t) = NS(t) + iEW(t), \quad (2)$$

where $NS(t)$ and $EW(t)$ are the signals from the NS and EW antennas, respectively, and $i = \sqrt{-1}$, then applying the Fourier transform

$$F(\omega) = \int_{-\infty}^{\infty} f(t)e^{-i\omega t}dt, \quad (3)$$

we can rewrite the resulting frequency domain signal as

$$F(\omega) = r_+ e^{i\theta_+} \qquad F(-\omega) = r_- e^{i\theta_-}. \quad (4)$$

[10] The major (A) and minor (B) axes of the polarization ellipse can now be expressed as

$$A = r_+ + r_- \qquad B = |r_+ - r_-|, \quad (5)$$

while the azimuth (ϕ) and eccentricity (ecc) of the ellipse can be written as

$$\phi = \frac{\theta_+ - \theta_-}{2} \qquad \text{ecc} = \sqrt{1 - \frac{B^2}{A^2}}. \quad (6)$$

[11] The azimuth of the polarization ellipse is equivalent to the azimuth that would be measured by a goniometer receiver and hence suffers from the same polarization and multipath error [*Yearby and Smith*, 1994]. *Strangeways* [1980] and *Strangeways and Rycroft* [1980] investigated the limitations of direction-finding techniques and found
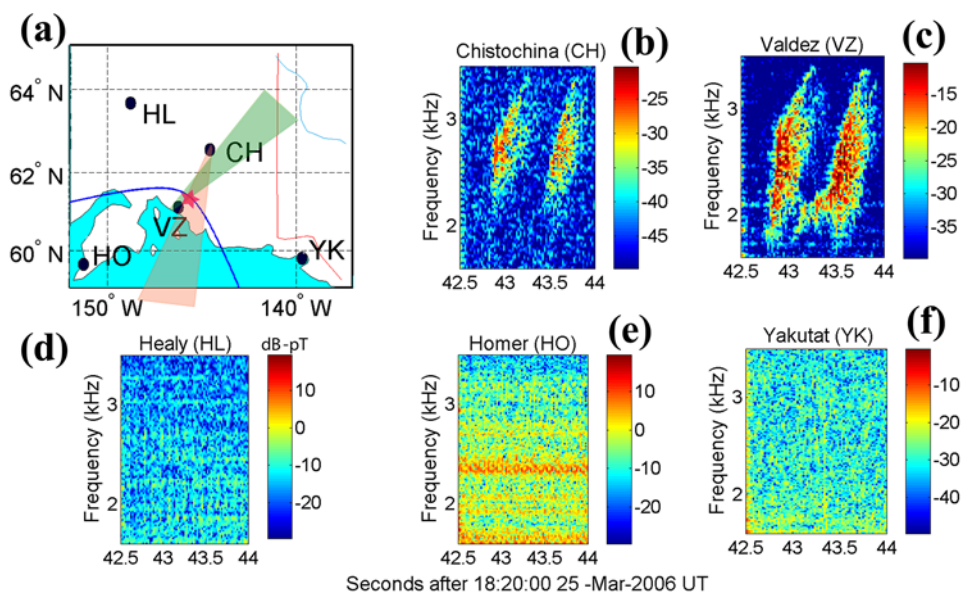
Figure 3. (a) Map showing exit point location with time of arrival delay curve (blue) and arrival azimuth from CH and VZ. Chorus risers observed exclusively at two sites: (b) CH and (c) VZ. No emissions were observed at (d) HL, (e) HO, or (f) YK.

that even if polarization and multipath errors are individually tens of degrees, the combined error is less than $10°$ if averaged over a 2 kHz bandwidth. The goniometer technique and the equivalent polarization ellipse decomposition used here are applicable for distances as short as 50 km from the source [*Strangeways and Rycroft*, 1980]. At these short distances the systematic error actually decreases, but measurement error arises since the polarization ellipse is nearly circular, as expected for whistler mode waves exiting the magnetosphere. In this context, the eccentricity expressed in equation (5) provides a measure of the degree of circular polarization and provides an additional diagnostic of the proximity of the ionospheric exit point. To obtain an arrival bearing for a chorus emission, an amplitude-weighted average of the polarization ellipse azimuth was calculated for the entire bandwidth of the emission.

3. Chorus Emissions With Singular Exit Points

[12] Discrete chorus emissions in Alaska show maximum activity and intensity around local noon. Analysis of several observations at multiple sites yielded the location of singular ionospheric exit points for the emissions. Figure 3 shows an example from 25 March 2006 where chorus emissions were observed exclusively at two sites, Chistochina (CH) and Valdez (VZ). Figures 3b and 3c show spectra from CH and VZ showing the same two frequency risers observed at both sites, while Figures 3d–3f show the lack of observation at Healy (HL), Homer (HO), and Yakutat (YK). Figure 3a shows a map of the sites as well as the location of the ionospheric exit point on the basis of the intersection of the time of arrival delay curve and the arrival azimuth beams from CH and VZ. The time of arrival lag for the direct ray between CH and VZ was 0.48 ms with a correlation coefficient of 0.58. The width of the intersecting shapes reflects the typical uncertainty levels in the measurements, approximately 10–30 km for time of arrival

delay and $\sim 10°$ for arrival azimuth. On the day of the observations, emissions very similar to the ones shown in Figure 3 continued to be observed for over an hour. During this time the exit point exhibited a magnetic northward drift of about 50 km. The analysis of several cases similar to that presented in Figure 3 allowed for determination of the typical propagation dynamics and spatial attenuation of the emissions. In the vicinity (<50 km) of the ionospheric exit point, chorus waves were found to have low eccentricity (0.4–0.8), indicative of near-circular polarization, as expected for whistler mode propagation in the magnetosphere. Moving away from the exit point, the quasi-transverse electromagnetic waveguide mode was preferentially excited, with significant mode coupling to the first quasi-transverse electric (QTE_1) mode occurring at distances over 100 km. In ray theory the QTE mode corresponds to rays with magnetic field in the plane of propagation. The spatial attenuation of the emissions in the waveguide depends on the propagation modes. Figure 4 shows spatial attenuation for three different chorus risers observed on 25 March 2006 as a function of distance from the ionospheric exit point. Each line in Figure 4 is a best fit of the amplitudes of three observations at a given frequency where each amplitude has been scaled to its maximum observed value at the site nearest the exit point. We find that for the higher frequencies ($\sim$3 kHz), which more rapidly couple to the QTE_1 mode, the attenuation rate is $\sim$9 dB/100 km and is comparable with the work by *Tsuruda et al.* [1982], who report an $\sim$7 dB/100 km attenuation rate. Lower frequencies ($\sim$2 kHz) exhibit a higher attenuation rate.

4. Chorus Emissions With Multiple Exit Points
4.1. Observations

[13] Despite comparable signal-to-noise ratios, for several emissions observed at multiple sites, single ionospheric exit point solutions satisfying the observed signal characteristics
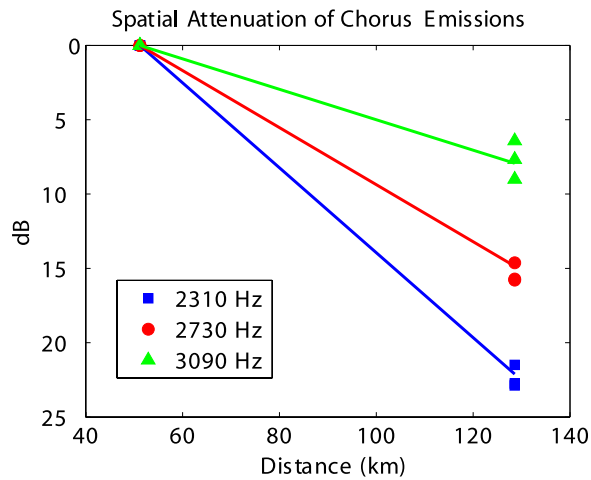
Figure 4. Spatial attenuation of chorus emissions with single exit points for three different frequency bands of three risers observed on 25 March 2006. Distance is measured relative to the ionospheric exit point and is normalized to the maximum observed value.

could not be found. In fact, analysis of isolated subsets of the observations yielded a large geographic spread of potential exit points. Figure 5 shows an example from 15 February 2007 where a series of five chorus risers are observed at CH, VZ, YK, and Juneau (JU) but not at Kodiak (KO). The maximum distance between these sites is 700 km, making a single exit point model incompatible with the attenuation rates of *Tsuruda et al.* [1982] and of those inferred in our study, as discussed in Section 3. Figure 5f shows that the attenuation rate with distance for an assumed singular exit point is much less than 7 dB/100 km. Further evidence against a single subionospheric source for the emissions is the fine spectral feature differences that cannot be the result of propagation in the Earth-ionosphere wave-

guide. For the case presented in Figure 5, it is determined that a model of chorus impinging on the ionosphere over an L shell range of $4 < L < 5$ best fits the observations. In effect, the chorus emissions observed at each site originate directly above (or in close proximity to) each receiver station. Such a propagation scheme explains the fine spectral feature differences between the emissions which may be due to differences in refraction (or absorption) through different local ionospheric conditions and is also supported by the fact that chorus emissions are not observed at KO, which is south of the $L = 4$ magnetic field line (see map in Figure 1).

4.2. Ray Tracing Analysis

[14] Significant coupling of whistler mode wave energy from the magnetosphere into the Earth-ionosphere wave-guide is impeded by the sharp index of refraction gradient at the Earth-ionosphere boundary, which causes waves at oblique wave normal angles with respect to the vertical (δ) to experience total internal reflection. The index of refraction of whistler mode waves, $\mu(\theta_k)$, is $>\sim 20-30$ in the ionosphere and is unity below the ionosphere, where θ_k is the wave normal angle with respect to the geomagnetic field. Only waves for which $\mu(\theta_k) \sin(\delta) < 1$ will not experience total internal reflection and will penetrate to the ground. Solving the above expression for δ and noting that for our observation latitudes the inclination of the geomag-netic field is $\sim 15°$, we obtain that $\theta_k < \sim 17°-18°$. It is straightforward to show that the above condition only allows penetration to the ground for θ_k tilted toward the equator [*Sonwalkar and Harikumar*, 2000], thus creating an effectively one-sided "ionospheric penetration cone." The requirement for waves to be in the ionospheric penetration cone in order to be observed on the ground has been the primary reason for the conventional thinking that magneto-spheric emissions observed on the ground are limited to those waves which propagated in field-aligned ducts since such guided propagation results in a near-vertical wave normal angle at the ionospheric altitudes. The multiple exit
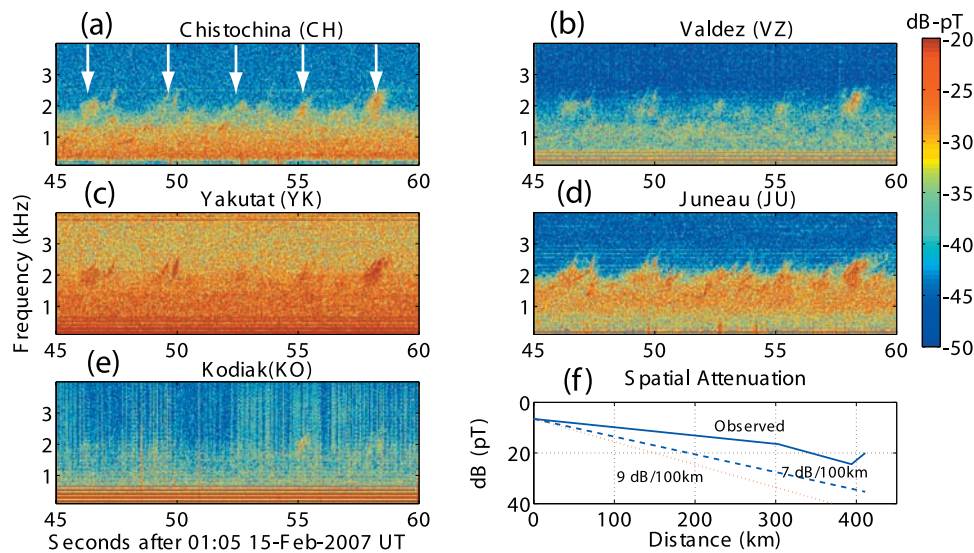

Figure 5. Five discrete chorus emissions with multiple exit points observed at (a) CH, (b) VZ, (c) YK, and (d) JU but not at (e) KO. (f) Spatial attenuation assuming a single exit point at YK with expected attenuation curves of 7 and 9 dB/100 km.

point observations presented in this study are unlikely to be ducted chorus waves since such a circumstance would require a concentration (or bundling) of ducts much greater than previously estimated [*Carpenter and Šulić*, 1988].

[15] Nonducted propagation of chorus whose wave normal vector remains field aligned and hence allows for penetration to the ground has recently been investigated theoretically by several authors. *Chum and Santolík* [2005] show that for an equatorial source a wave normal angle close to the Gendrin angle can yield ray trajectories that reach the topside ionosphere with $\theta_k \sim 0$. *Bortnik et al.* [2007] show similar results for different conditions and also incorporate Landau damping, illustrating that such field-aligned waves are minimally damped along their trajectory from equator to ionospheric boundary. While our ground-based observations seem to offer a confirmation of the above theoretical works, such a conclusion is only partially satisfying since both *Chum and Santolík* [2005] and *Bortnik et al.* [2007] use specific cold plasma density models that do not necessarily apply to our observations. *Bortnik et al.* [2007] perform ray tracing in a highly disturbed magnetosphere with plasmapause located at $L \sim 2.5$, while *Chum and Santolík* [2005] do not include a plasmapause boundary at all. On the day of our multiple exit point observations (15 February 2007) the plasmapause boundary was at $L = 3.8$, as derived from the Kp index using the formulations of *Carpenter and Anderson* [1992].

[16] In order to explore nonducted propagation modes under conditions approximating those of our observations, we performed magnetospheric ray tracing using the 2-dimensional Stanford ray tracing code [*Inan and Bell*, 1977]. The goal of the analysis was to determine the viability of a source that would reproduce the observations of chorus penetrating the ionosphere over the span $4 < L < 5$ for a magnetosphere with plasmapause close to $L = 3.8$ but devoid of additional guiding structures. The Stanford ray tracing code uses a diffusive equilibrium model [*Angerami and Thomas*, 1964] and a dipole magnetic field and is the same propagation code as that used by *Bortnik et al.* [2007], except that we have not incorporated Landau damping since we are interested primarily in propagation trajectories and less so in the wave amplitude along said trajectories. Raypaths were calculated for all propagating wave normal angles and source regions spanning $3.8 < L < 6.5$ (source regions outside the plasmapause) with $\Delta L = 0.05L$ and $\Delta\theta_{k0} = 0.2°$. Since the chorus source region has been confirmed to be within a few degrees of the magnetic equator [*Santolík and Gurnett*, 2003; *LeDocq et al.*, 1998], all rays were launched from the equator. A calculated ray trajectory was deemed consistent with the observations if the trajectory arrived to an altitude of less than 1000 km in the L shell range of $4 < L < 5$ with wave normal angle within the ionospheric penetration cone. Although a more thorough treatment would require the additional verification that a consistent ray is not completely extinguished by Landau damping, *Bortnik et al.* [2007] show that ray trajectories which penetrate to the ground are minimally damped. In general, the roughly field aligned raypath required for a consistent ray will minimize Landau damping, which is maximum for oblique propagation. Our neglect of Landau damping is thus appropriate for our limiting case study.

[17] The initial simulation with plasmapause located at $L_{pp} = 3.8$ did not yield any rays consistent with the observations. Repeating the simulation with the plasmapause boundary located at $L_{pp} = 4.0$, representing a less disturbed magnetosphere, likewise did not produce any consistent rays. Exploring more disturbed conditions, we find consistent rays when the plasmapause location is moved substantially inward to $L_{pp} = 3.0$ and $L_{pp} = 2.75$. The consistent rays for the $L_{pp} = 3.0$ plasmapause case originate near and are partially guided by the plasmapause boundary which is known to act as an effective waveguide [*Inan and Bell*, 1977]. The consistent rays for the $L_{pp} = 2.75$ case are similar to the *Bortnik et al.* [2007] results in that the initial wave normal angles have magnitudes of around 80% of the Gendrin angle tilted toward the Earth and source location such that $f/f_c \sim 0.15$, where f_c is the electron gyrofrequency. However, we find neither of these two disturbed profiles ($L_{pp} = 2.75$ and $L_{pp} = 3.0$) to be realistic representations of the conditions for our observations since they require Kp_{max} of 5.7 and 6.3 [*Carpenter and Anderson*, 1992], while the Kp_{max} for our observations is 4.3. It becomes apparent that the location of the plasmapause seems to play a significant role in whether ray trajectories are able to penetrate the ionosphere. It is possible that the magnetospheric cold plasma density on the day of our observations was not as simple as is assumed under typical models, especially at higher latitudes. It is also important to note that predictions of the plasmapause location based on magnetic indices generally can involve uncertainties on the order of $0.7-0.9 \, L$ [*O'Brien and Moldwin*, 2003]. *Chum and Santolík* [2005] postulate that the plasmapause is only weakly expressed at higher latitudes, making it more likely for field-aligned rays to reach the topside of the ionosphere. Another inadequacy of attempting to match the ground observations with ray tracing simulations is the latter's inherent inability to handle small-scale irregularities, which are known to be prevalent at altitudes less than 1000 km [*Dyson*, 1969; *Clark and Raitt*, 1976; *Gross and Muldrew*, 1984].

[18] Of particular relevance in this connection is the work of *Sonwalkar and Harikumar* [2000], who set out to explain ground observations of auroral hiss over wide spatial ranges. The authors found that meter-scale (1–100 m) irregularities at altitudes <5000 km played a key role in scattering (via linear mode conversion) the large wave normal angles to small ones within the ionospheric penetration cone. Using a code initially developed by *Bell and Ngo* [1990] for modeling whistler mode scattering from magnetic-field-aligned density irregularities, *Sonwalkar and Harikumar* [2000] show that passive linear scattering from irregularities with relative density enhancements from 10 to 50% can cause conversion from high θ_k to low θ_k (<~10°) with up to 10% power efficiency. Scattering from such small-scale irregularities could be another missing link between our ground observations and the lack of penetrating ray trajectories for our expected plasmapause location.

5. Chorus-Induced Electron Precipitation

5.1. Observations of VLF Precipitation Signatures

[19] The role of chorus in the precipitation and acceleration of energetic electrons and controlling radiation belt dynamics is a topic of active study [*O'Brien et al.*, 2003;
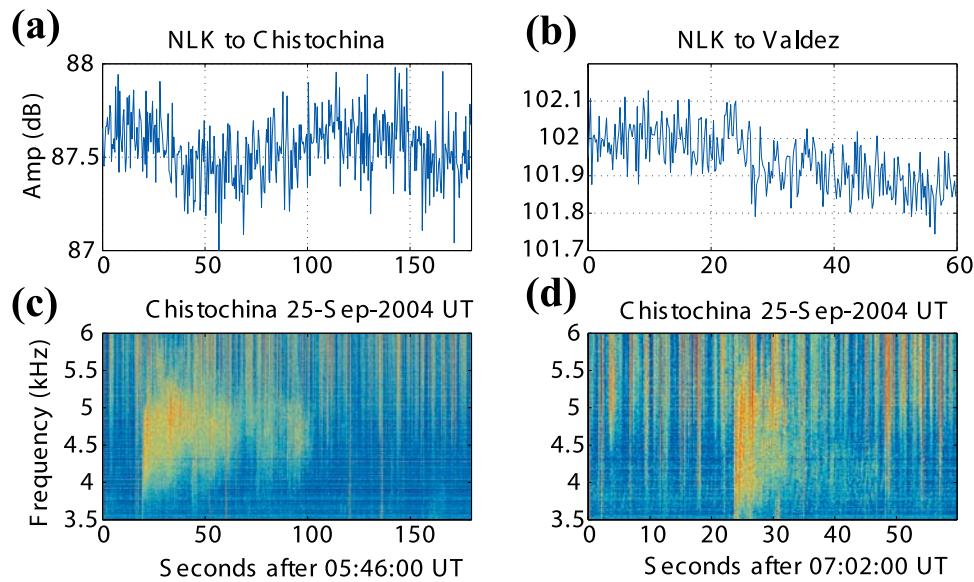
Figure 6. (a, b) Two cases of VLF amplitude responses on the NLK transmitter to (c, d) whistler-triggered chorus emissions observed at Chistochina.

Bortnik and Thorne, 2007]. The ability to geolocate exit points of chorus emissions (when such single exit points exist) suggests that simultaneous ground observations of both chorus emissions and particle precipitation can be correlated and used as a complement to satellite measurements. Although ground-based measurements can be more complicated to interpret, they offer the advantages of wide spatial coverage and continuous long-term recordings. In particular the VLF remote sensing technique allows for the

realization of ground-based particle precipitation measurements over large geographic areas with only a few receivers.

[20] The VLF remote sensing technique utilized in this study allows the detection of ionospheric perturbations caused by energetic electron precipitation via corresponding changes in the amplitude and phase of subionospherically propagating VLF transmitter signals in the ~20–30 kHz range. This technique is particularly suited for detection of precipitating electrons with energies greater than 50 keV.
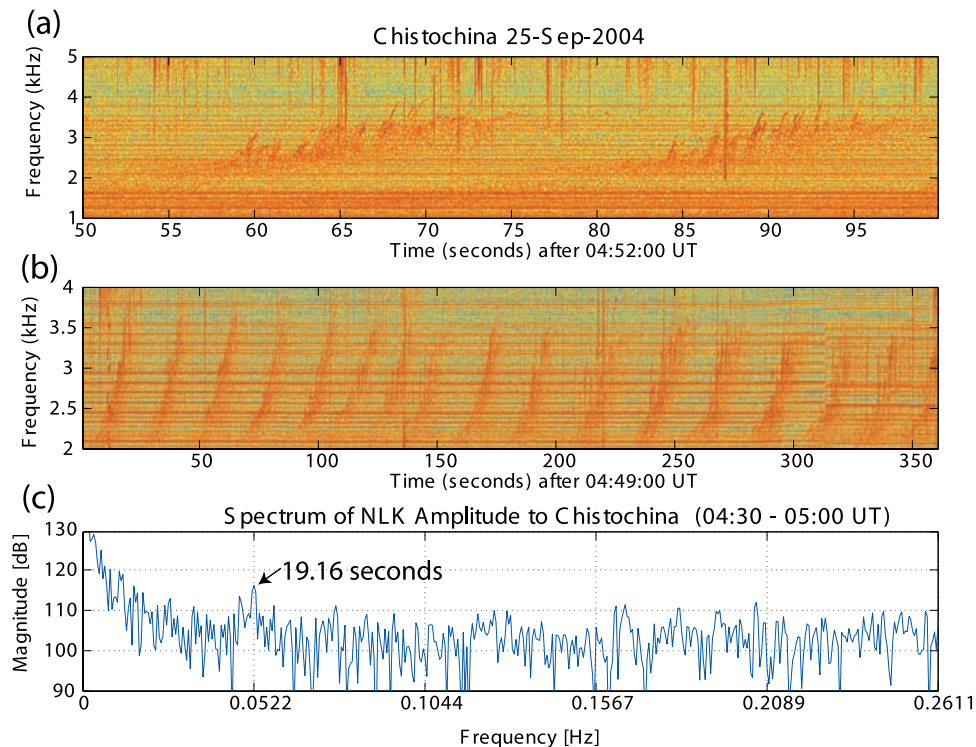

Figure 7. (a, b) QP emissions observed at Chistochina showing ~19 s periodicity. (c) Spectrum of NLK amplitude received at Chistochina showing periodicity of 19.16 s (0.0522 Hz).

While VLF remote sensing is a powerful tool for detecting energetic electron precipitation, it can primarily be used only at nighttime since the ambient electron densities at the VLF reflection height during daytime are too high compared to the secondary ionization changes produced by relatively weak chorus-induced electron precipitation bursts. As a result, we cannot use this method to measure precipitation for most of the more intense chorus emission cases (including the earlier examples presented in sections 3 and 4), which at the location of our observations tend to occur during daylight hours.

[21] We focus here instead on the observations from 25 September 2004, a particularly active day with a rich variety of magnetospheric emissions continuing well into nighttime. Figures 6a and 6b show two cases of observations of precipitation bursts in correlation with whistler-triggered chorus emissions (Figures 6c and 6d) observed at Chistochina in the 3.5–6 kHz band. For both events the amplitude of the 24.8 kHz NLK transmitter signal from Jim Creek, Washington, shows an ∼0.4 dB amplitude change corresponding to the observed chorus emissions. In Figure 6a the amplitude change is shown to occur on the path to CH, while in Figure 6b the amplitude change occurs on the more southerly path to VZ, as seen in Figure 1.

[22] While the precipitation fluxes from whistler-triggered events on this day were large enough to generate individually discernible VLF perturbations, the precipitation signatures of other emissions required averaging to be detected. Figure 7 shows an example where quasi-periodic (QP) emissions were observed with a period of ∼19 s. QP emissions are understood to be composed of discrete chorus emissions with an additional mechanism, most likely related to geomagnetic pulsations, responsible for the quasi-periodic nature [*Sato et al.*, 1981; *Sazhin and Hayakawa*, 1994]. Figures 7a and 7b show spectra of the emissions on different timescales, while Figure 7c shows a Fourier spectrum of the amplitude of the NLK signal to Chistochina. The amplitude spectrum shows a clear peak at 0.0522 Hz corresponding to a 19.16 s period. Hence even though the individual precipitation signatures produced by the QP emissions were weak, their periodicity facilitates their detection. Superposed epochs of these signatures are also calculated and show time signatures similar to those of the whistler-triggered events in Figure 6.

5.2. Discussion

[23] The recovery rate back to ambient level of a VLF perturbation is primarily a function of atmospheric chemistry and hence the altitude range where the ionospheric perturbation occurs [*Pasko and Inan*, 1994]. The altitude of the perturbation in turn depends on the energy of the precipitating electron fluxes. The recovery rate for perturbations caused by 50–300 keV electrons (deposited at 75–85 km) is on the order of seconds to tens of seconds [*Inan et al.*, 1988a, 1988b]. Relativistic electrons with energies around 1 MeV, on the other hand, are deposited as low as 60 km and have recovery rates less than a second [*Inan et al.*, 1988a, 1988b; *Lehtinen et al.*, 2001].

[24] The recovery signatures observed on the events shown in Figure 6 are on the order of 10 s and hence are likely dominated by nonrelativistic (i.e., <1 MeV) precipi-

tation fluxes. This result is consistent with theoretical gyroresonance modeling of chorus-induced precipitation such as that of *Bortnik and Thorne* [2007] which shows peak fluxes of 100–300 keV electrons. *Bortnik and Thorne* [2007] also predict simultaneous microbursts of >1 MeV electrons, and it is possible that in our observations this relativistic energy signature is buried under the dominant lower-energy response. Nonetheless, we do not observe the inferred exclusively relativistic (>1 MeV) response (<1 s recovery) reported by *Rodger et al.* [2007].

6. Summary

[25] We take advantage of GPS timing accuracy on multiple receivers to accurately locate chorus emission exit points for the first time. While we verify many aspects of past work, an exciting new finding is the observation of chorus emissions on the ground that apparently did not propagate solely in magnetospheric ducts. While our observations suggest confirmation of the modeling work of *Chum and Santolík* [2005] and *Bortnik et al.* [2007], it must be noted that the magnetospheric density models used by these authors do not reflect those expected for our observations on the basis of geomagnetic conditions. Ray tracing analysis performed in this study illustrates that either the magnetospheric density model used in the code is inadequate or linear scattering/mode conversion from irregularities is involved in the multiexit point chorus observations. Simultaneous observations of multiexit point chorus with radar observations of irregularities would serve to quantify the relationship, although the irregularities in question here might well be at high altitudes (∼5000 km) beyond the range of radars. Since chorus waves propagating in the nonducted mode are apparently observable on the ground, it is possible that some of the unexplained effects in past observations may now be better understood. In particular, the fast fluctuations of amplitude and arrival azimuth reported by *Carpenter* [1980] or the rapid exit point changes reported by *Madden et al.* [1978] might be explained by including nonducted propagation and scattering from irregularities. Our observations of chorus-induced electron precipitation indicate that the associated precipitation bursts are dominated by nonrelativistic (<1 MeV) electrons. In future work it is planned to utilize the exit point location in conjunction with VLF remote sensing to quantify precipitation by ducted chorus emissions.

References

Angerami, J. J., and J. O. Thomas (1964), Studies of planetary atmospheres: 1. Distribution of electrons and ions in the Earth's exosphere, *J. Geophys. Res.*, 69(21), 4537–4560.
Bell, T. F., and H. D. Ngo (1990), Electrostatic lower hybrid waves excited by electromagnetic whistler mode waves scattering from planar magnetic-field-aligned plasma density irregularities, *J. Geophys. Res.*, 95(A1), 149–172.

Bortnik, J., and R. M. Thorne (2007), The dual role of ELF/VLF chorus waves in the acceleration and precipitation of radiation belt electrons, *J. Atmos. Sol. Terr. Phys.*, 69, 378–386.

Bortnik, J., R. M. Thorne, N. P. Meredith, and O. Santolik (2007), Ray tracing of penetrating chorus and its implications for the radiation belts, *Geophys. Res. Lett.*, 34, L15109, doi:10.1029/2007GL030040.

Carpenter, D. L. (1980), Fast fluctuations in the arrival bearing of magnetospherically propagating signals from the Siple, Antarctica, VLF transmitter, *J. Geophys. Res.*, 85(A8), 4157–4166.

Carpenter, D. L., and R. R. Anderson (1992), An ISEE/whistler model of equatorial electron density in the magnetosphere, *J. Geophys. Res.*, 97(A2), 1097–1108.

Carpenter, D. L., and D. M. Šulić (1988), Ducted whistler propagation outside the plasmapause, *J. Geophys. Res.*, 93(A9), 9731–9742.

Chum, J., and O. Santolík (2005), Propagation of whistler-mode chorus to low altitides: Divergent ray trajectories and ground acessibility, *Ann. Geophys.*, 23, 3727–3738.

Clark, D. H., and W. I. Raitt (1976), The global morphology of irregularities in the topside ionosphere, as measured by the total ion current probe on ESRO-4, *Planet. Space Sci.*, 24(9), 873–881.

Cousins, M. D. (1972), Direction finding on whistlers and related VLF signals, *Tech. Rep. 34432-2*, Space, Telecommun., and Radiosci. Lab., Stanford Univ., Calif.

Dingle, B., and D. L. Carpenter (1981), Electron precipitation induced by VLF noise bursts at the plasmapause and detected at conjugate ground stations, *J. Geophys. Res.*, 86(A6), 4597–4606.

Dyson, P. L. (1969), Direct measurements of the size and amplitude of irregularities in the topside ionosphere, *J. Geophys. Res.*, 74(26), 6291–6303.

Gross, S. H., and D. B. Muldrew (1984), Uniformly spaced field-aligned ionization ducts, *J. Geophys. Res.*, 89(A10), 8986–8996.

Hayakawa, M., Y. Tanaka, A. Iwai, J. Ohtsu, L. R. O. Storey, C. Beghin, and T. S. Jorgensen (1981), Simultaneous spaced direction-finding measurements of medium-latitude VLF/ELF emissions, *Planet. Space Sci.*, 29(5), 505–520.

Inan, U. S., and T. F. Bell (1977), The plasmapause as a VLF wave guide, *J. Geophys. Res.*, 82(19), 2819–2827.

Inan, U. S., T. G. Wolf, and D. L. Carpenter (1988a), Geographic distribution of lightning-induced electron precipitation observed as VLF/LF perturbation events, *J. Geophys. Res.*, 93(A9), 9841–9853.

Inan, U. S., W. C. Burgess, T. G. Wolf, D. C. Shafer, and R. E. Orville (1988b), Lightning-associated precipitation of MeV electrons from the inner radiation belt, *Geophys. Res. Lett.*, 15(2), 172–175.

Inan, U. S., M. Platino, T. F. Bell, D. A. Gurnett, and J. S. Pickett (2004), Cluster measurements of rapidly moving sources of ELF/VLF chorus, *J. Geophys. Res.*, 109, A05214, doi:10.1029/2003JA010289.

Inan, U. S., M. Golkowski, M. K. Casey, R. C. Moore, W. Peter, P. Kulkarni, P. Kossey, E. Kennedy, S. Meth, and P. Smit (2007), Subionospheric VLF observations of transmitter-induced precipitation of inner radiation belt electrons, *Geophys. Res. Lett.*, 34, L02106, doi:10.1029/2006GL028494.

Lauben, D. S., U. S. Inan, T. F. Bell, and D. A. Gurnett (2002), Source characteristics of ELF/VLF chorus, *J. Geophys. Res.*, 107(A12), 1429, doi:10.1029/2000JA003019.

Leavitt, M. K., D. L. Carpenter, N. T. Seely, R. R. Padden, and J. H. Doolittle (1978), Initial results from a tracking receiver direction finder for whistler mode signals, *J. Geophys. Res.*, 83(A4), 1601–1610.

LeDocq, M. J., D. A. Gurnett, and G. B. Hospodarsky (1998), Chorus source locations from VLF Poynting flux measurements with the polar spacecraft, *Geophys. Res. Lett.*, 25(21), 4063–4066.

Lee, A. C. L. (1986), An operational system for the remote location of lightning flashes using a VLF arrival time difference technique, *J. Atmos. Oceanic Technol.*, 3, 630–642.

Lehtinen, N. G., U. S. Inan, and T. F. Bell (2001), Effects of thunderstorm-driven runaway electrons in the conjugate hemisphere: Purple sprites, ionization enhancements, and gamma rays, *J. Geophys. Res.*, 106(A12), 28,841–28,856.

Lorentzen, K. R., J. B. Blake, U. S. Inan, and J. Bortnik (2001), Observations of relativistic electron microbursts in association with VLF chorus, *J. Geophys. Res.*, 106(A4), 6017–6028.

Madden, M. A., M. J. Rycroft, and N. E. Smith (1978), Ground-based ELF/VLF observations at high latitudes during passes of GEOS-1 and ISEE-1 and -2, *Space Sci. Rev.*, 22, 465–479.

Neudegg, D. A., B. J. Fraser, F. W. Menk, H. J. Hansen, G. B. Burns, R. J. Morris, and M. J. Underwood (1995), Sources and velocities of Pc1-2 ULF waves at high latitudes, *Geophys. Res. Lett.*, 22(21), 2965–2968.

O'Brien, T. P., and M. B. Moldwin (2003), Empirical plasmapause models from magnetic indices, *Geophys. Res. Lett.*, 30(4), 1152, doi:10.1029/2002GL016007.

O'Brien, T. P., K. R. Lorentzen, I. R. Mann, N. P. Meredith, J. B. Blake, J. F. Fennell, M. D. Looper, D. K. Milling, and R. R. Anderson (2003), Energization of relativistic electrons in the presence of ULF power and MeV microbursts: Evidence for dual ULF and VLF acceleration, *J. Geophys. Res.*, 108(A8), 1329, doi:10.1029/2002JA009784.

Pasko, V. P., and U. S. Inan (1994), Recovery signatures of lightning-associated VLF perturbations as a measure of the lower ionosphere, *J. Geophys. Res.*, 99(A9), 17,523–17,538.

Peter, W. B., and U. S. Inan (2004), On the occurrence and spatial extent of electron precipitation induced by oblique nonducted whistler waves, *J. Geophys. Res.*, 109, A12215, doi:10.1029/2004JA010412.

Rodger, C. J., M. A. Clilverd, D. Nunn, P. T. Verronen, J. Bortnik, and E. Turunen (2007), Storm time, short-lived bursts of relativistic electron precipitation detected by subionospheric radio wave propagation, *J. Geophys. Res.*, 112, A07301, doi:10.1029/2007JA012347.

Rosenberg, T. J., J. C. Siren, D. L. Matthews, K. Marthinsen, J. A. Holtet, A. Egeland, D. L. Carpenter, and R. A. Helliwell (1981), Conjugacy of electron microbursts and VLF chorus, *J. Geophys. Res.*, 86(A7), 5819–5832.

Santolík, O., and D. A. Gurnett (2003), Transverse dimensions of chorus in the source region, *Geophys. Res. Lett.*, 30(2), 1031, doi:10.1029/2002GL016178.

Sato, N., H. Fukunishi, T. Ozaki, and T. Yoshino (1981), Simultaneous ground-satellite observations of quasi-periodic (QP) ELF-VLF emissions near L = 6, *J. Geophys. Res.*, 86(A12), 9953–9960.

Sazhin, S. S., and M. Hayakawa (1992), Magnetopsheric chorus emissions: A review, *Planet. Space Sci.*, 40(5), 681–697.

Sazhin, S. S., and M. Hayakawa (1994), Periodic and quasiperiodic VLF emissions, *J. Atmos. Terr. Phys.*, 56, 735–753.

Sonwalkar, V. S., and J. Harikumar (2000), An explanation of ground observations of auroral hiss: Role of density depletions and meter-scale irregularities, *J. Geophys. Res.*, 105(A8), 18,867–18,884.

Storey, L. R. O. (1953), An investigation of whistling atmospherics, *Philos. Trans. R. Soc. London, Ser. A*, 246, 113–141.

Strangeways, H. J. (1980), Systematic errors in VLF direction-finding of whistler ducts—I, *J. Atmos. Terr. Phys.*, 42, 995–1008.

Strangeways, H. J., and M. J. Rycroft (1980), Systematic errors in VLF direction-finding of whistler ducts—II, *J. Atmos. Terr. Phys.*, 42, 1009–1023.

Strangeways, H. J., M. J. Rycroft, and M. J. Jarvis (1982), Multi-station VLF direction-finding measurements in eastern Canada, *J. Atmos. Terr. Phys.*, 44, 378–386.

Tsuruda, K., and K. Hayashi (1974), A new method for direction finding of elliptically polarized VLF waves, *Rep. 509*, Inst. of Space and Aeronaut. Sci., Univ. of Tokyo, Japan.

Tsuruda, K., S. Machida, T. Teresawa, and A. Nishida (1982), High spatial attenuation of the siple transmitter signal and natural VLF chorus observed at ground-based chain stations near Roberval, Quebec, *J. Geophys. Res.*, 87(A2), 742–750.

Yearby, K. H., and A. J. Smith (1994), The polarisation of whistlers received on the ground near L = 4, *J. Atmos. Terr. Phys.*, 56, 1499–1512.

———————————
M. Gołkowski and U. S. Inan, STAR Laboratory, Stanford University, Stanford, CA 94305, USA. (mag41@stanford.edu)